Cardiovascular Research (2017) **113**, 531–541
doi:10.1093/cvr/cvx006

Elucidating arrhythmogenic mechanisms of long-QT syndrome *CALM1*-F142L mutation in patient-specific induced pluripotent stem cell-derived cardiomyocytes

Marcella Rocchetti[1†], Luca Sala[1,2†], Lisa Dreizehnter[3†], Lia Crotti[2,4], Daniel Sinnecker[3], Manuela Mura[4,5], Luna Simona Pane[3], Claudia Altomare[1], Eleonora Torre[1], Gaspare Mostacciuolo[1], Stefano Severi[6], Alberto Porta[7,8], Gaetano M. De Ferrari[4,5], Alfred L George Jr[9], Peter J. Schwartz[2], Massimiliano Gnecchi[4,5,10], Alessandra Moretti[3,11†], and Antonio Zaza[1,*†]

[1]Department of Biotechnology and Bioscience, University of Milano-Bicocca, Milan, Italy; [2]Center for Cardiac Arrhythmias of Genetic Origin and Laboratory of Cardiovascular Genetics, IRCCS Istituto Auxologico Italiano, Milan, Italy; [3]I. Medical Department - Cardiology, Klinikum Rechts der Isar- Technische Universität München, Munich, Germany; [4]Department of Molecular Medicine – Unit of Cardiology, University of Pavia, Pavia, Italy; [5]Department of Cardiothoracic and Vascular Sciences – Coronary Care Unit and Laboratory of Clinical and Experimental Cardiology, Fondazione IRCCS Policlinico San Matteo, Pavia, Italy; [6]Biomedical Engineering Laboratory D.E.I, University of Bologna, Cesena, Italy; [7]Department of Biomedical Sciences for Health, University of Milan, Milan, Italy; [8]Department of Cardiothoracic, Vascular Anesthesia and Intensive Care, IRCCS Policlinico San Donato, Milan, Italy; [9]Department of Pharmacology, Northwestern University Feinberg School of Medicine, Chicago, Illinois, USA; [10]Department of Medicine, University of Cape Town, Cape Town, South Africa; and [11]DZHK (German Centre for Cardiovascular Research) - Partner Site Munich Heart Alliance, Munich, Germany

Received 19 April 2016; revised 3 January 2017; editorial decision 11 January 2017; accepted 15 January 2017; online publish-ahead-of-print 2 February 2017

Time for primary review: 50 days

Aims Calmodulin (CaM) is a small protein, encoded by three genes (*CALM1-3*), exerting multiple Ca^{2+}-dependent modulatory roles. A mutation (F142L) affecting only one of the six *CALM* alleles is associated with long QT syndrome (LQTS) characterized by recurrent cardiac arrests. This phenotypic severity is unexpected from the predicted allelic balance. In this work, the effects of heterozygous *CALM1*-F142L have been investigated in human induced pluripotent stem cell-derived cardiomyocytes (hiPSC-CMs) obtained from a LQTS patient carrying the F142L mutation, i.e. in the context of native allelic ratio and potential gene modifiers.

Methods and Results Skin fibroblasts of the mutation carrier and two unrelated healthy subjects (controls) were reprogrammed to hiPSC and differentiated into hiPSC-CMs. Scanty I_{K1} expression, an hiPSC-CMs feature potentially biasing repolarization, was corrected by addition of simulated I_{K1} (Dynamic-Clamp). Abnormalities in repolarization rate-dependency (in single cells and cell aggregates), membrane currents and intracellular Ca^{2+} dynamics were evaluated as putative arrhythmogenic factors. *CALM1*-F142L prolonged repolarization, altered its rate-dependency and its response to isoproterenol. This was associated with severe impairment of Ca^{2+}-dependent inactivation (CDI) of I_{CaL}, resulting in augmented inward current during the plateau phase. As a result, the repolarization of mutant cells failed to adapt to high pacing rates, a finding well reproduced by using a recent hiPSC-CM action potential model. The mutation failed to affect I_{Ks} and I_{NaL} and changed I_f only marginally. Intracellular Ca^{2+} dynamics and Ca^{2+} store stability were not significantly modified. Mutation-induced repolarization abnormalities were reversed by verapamil.

Conclusion The main functional derangement in *CALM1*-F142L was prolonged repolarization with altered rate-dependency and sensitivity to β-adrenergic stimulation. Impaired CDI of I_{CaL} underlined the electrical abnormality, which was

* Corresponding author. Dipartimento di Biotecnologie e Bioscienze Università Milano-Bicocca, P.za della Scienza 2, 20126 Milano, Italy. Tel: +39 02 6448 3307; fax: +39 02 6448 3565, E-mail: antonio.zaza@unimib.it

† The first three authors and the last two authors contributed equally to the study.

sensitive to I_{CaL} blockade. High mutation penetrance was confirmed in the presence of the native genotype, implying strong dominance of effects.

Keywords LQTS • Calmodulin • Mutations • Sudden death • hiPSC-CMs

1. Introduction

The congenital long QT syndrome (LQTS) is a genetic disorder characterized by QT interval prolongation and by propensity to life-threatening arrhythmias.[1] We recently provided the first evidence of a malignant form of LQTS associated with calmodulin (CaM) mutations[2]; other reports of CaM mutations in arrhythmogenic syndromes have followed.[3–5] CaM is a small Ca^{2+}-binding protein essential for multiple signalling processes in eukaryotic cells.[6] Mammals have three CaM genes (*CALM1*, *2*, and *3*) that encode identical amino acid sequences.[7] In the heart, CaM transduces Ca^{2+} signals to regulate, either directly or through CaMKII, electrophysiology and Ca^{2+} handling.[8]

Ca^{2+}-binding affinity is variably altered by CaM mutations linked to arrhythmogenic syndromes. Whereas the LQTS phenotype prevails among those with reduced Ca^{2+} affinity, mutations with normal Ca^{2+} affinity are often associated with catecholaminergic polymorphic ventricular tachycardias (CPVT).[3,9,10]

In the setting of LQTS, heterologous expression of mutated *CALM* is associated with delayed I_{CaL} inactivation, prolonged repolarization and perturbed intracellular Ca^{2+} handling.[11,12] However, heterologous expression of mutant constructs cannot reproduce the amount and subcellular localization of the abnormal protein. Therefore, albeit unveiling mutation effects potentially involved in arrhythmogenesis, previous studies did not clarify whether these effects are truly present in mutation carriers and to which extent they may contribute to electrical instability.

The present study evaluates the effects of an heterozygous *CALM1*-F142L mutation with reduced Ca^{2+} affinity, first identified in a LQTS patient suffering multiple cardiac arrests since infancy,[2] using 'induced pluripotent stem cell-derived cardiomyocytes' (hiPSC-CMs) generated from patient's skin fibroblasts. This allowed to test mutation effects in the context of the patient's own genotype, including potential adaptive transcriptional or post-transcriptional remodelling. The results demonstrate that defective I_{CaL} inactivation is the dominant mutation consequence and suggest the resulting repolarization delay as the most likely arrhythmogenic effect.

2. Methods

The Ethical Committee of the Fondazione IRCCS Policlinico San Matteo approved the study, which was performed in accordance with the Declaration of Helsinki. All samples were collected after obtaining informed consent from the donors. The investigation conforms to the Guide of the Care and Use of Laboratory Animals (NIH publication No. 85-23, revised 2011) and to the guidelines for animal care endorsed by Università Milano-Bicocca. An expanded Methods section is available in the Supplementary material online.

2.1 Generation and differentiation of induced pluripotent stem cells

Human induced pluripotent stem cells (hiPSCs) were generated by Sendai virus-mediated reprogramming of dermal fibroblasts and differentiated into cardiac bodies (CB)[13] (see Supplementary material online, *Figures S1* and *S2* for details). For patch-clamp measurements, mature CBs were dissociated into single hiPSC-CMs and analysed within 3–5 days. The presence of the *CALM1*-F142L mutation was verified by PCR on skin fibroblasts, hiPSCs and hiPSC-CMs (see Supplementary material online, *Figure S1*, primer sequences in *Table S1*).

2.2 Molecular studies

Gene expression was quantified by qRT-PCR, the results were normalized to *GAPDH*. Total CaM protein level was quantified by densitometric analysis of western blots. CaMKII activity was measured in hiPSC-CMs by a FRET assay based on the biosensor Camui-CR[14] cloned into a lentiviral vector.

2.3 Electrical activity in multicellular preparations and single cells

Extracellular field-potentials were recorded at 37 °C in spontaneously beating CBs by Multiple Electrode Array (MEA). Field-potential duration, reflecting electrical systole, was measured from the onset of the sharp positive deflection to the peak of the secondary slow deflection[15]; for simplicity, we will refer to this measurement as QT, which was rate-corrected (QTc) by Bazett's formula. CBs contraction was recorded with a Video Edge detection System.

Action potentials (APs) were recorded by whole-cell patch-clamp in hiPSC-CM paced at 0.5, 1, 2, and 3.3 Hz during Tyrode superfusion (36.5 °C). Under native conditions, hiPSC-CM had partially depolarized diastolic potentials (E_{diast} -50.5 ± 3.7 mV at 0.5 Hz), a likely consequence of low I_{K1} expression in immature myocytes.[16] Thus, numerically modelled I_{K1}[17] (see Supplementary material online, *Table S2*) was injected in the hiPSC-CM by Dynamic Clamp (DC).[18,19] AP measurements under DC are described in the manuscript, those in native conditions in the Supplementary material online.

2.4 Characterization of membrane currents

I_{CaL} was recorded in voltage-clamped hiPSC-CMs at room temperature to minimize current rundown. Peak *I/V* relationships, steady-state activation/inactivation, and recovery kinetics were obtained by standard protocols (detail in Supplementary material online); mid activation/inactivation potential ($V_{0.5}$) and the reciprocal slope factors (k, in mV) were estimated by Boltzmann fitting. The magnitude of I_{CaL} 'window', defined as the overlap of steady-state activation and inactivation curves, was quantified (*Table 1*) as overlap area (Area), voltage (V@Peak) and open probability at curves intersection (Po_{max}). To quantify Ca^{2+}-dependent inactivation (CDI), I_{CaL} was recorded, within each cell, with Ca^{2+} (I_{CaL}) or equimolar Ba^{2+} (I_{BaL}) as charge carriers. CDI was expressed as the difference between I_{BaL} and I_{CaL} at 100 ms (r_{100}) and 300 ms (r_{300}). Rate-dependent I_{CaL} facilitation (CDF) was measured at 36.5 °C, as progressive enhancement of I_{CaL} (measured during the first 50 ms of the activating step) following initiation of repetitive activations at 0.05 and 1 Hz.

Table 1 Comparison of I_{CaL} parameters between CTR1 and the *CALM1*-F142L c1 and c2 clones separately

	CTR1	F142L			
		c1	*P* vs. CTR1	c2	*P* vs. CTR1
Activation curve					
$V_{0.5}$ (mV)	-11.3 ± 0.78	-9.9 ± 1.12	NS	-8.9 ± 1.42	NS
k (mV)	6.7 ± 0.27	7.7 ± 0.31	<0.05	7.8 ± 0.35	<0.05
G_{max} (nS/pF)	0.22 ± 0.03	0.25 ± 0.03	NS	0.26 ± 0.05	NS
Inactivation curve					
$V_{0.5}$ (mV)	-30.2 ± 0.62	-27.8 ± 0.7	<0.05	-28.1 ± 0.8	<0.05
k (mV)	4.8 ± 0.29	5.5 ± 0.29	NS	5.8 ± 0.16	<0.05
G_{min}/G_{max}	0.03 ± 0.005	0.09 ± 0.01	<0.05	0.08 ± 0.01	<0.05
Window					
Area (a.u.)	2.9 ± 0.34	5.2 ± 0.36	<0.05	4.8 ± 0.78	<0.05
V@Peak (mV)	-21.9 ± 0.84	-17.8 ± 0.86	<0.05	-19.2 ± 1.4	NS
Po_{max} (10^{-3})	31.6 ± 3.8	64.7 ± 4.4	<0.05	62.0 ± 11.5	<0.05

$V_{0.5}$, mid activation/inactivation potential; *k*, reciprocal slope factor (in mV) of activation/inactivation curves; G_{max} = maximal conductance; Area, 'window' area (in arbitrary units); *V*@Peak = membrane potential at which activation and inactivation curves intersect; Po_{max}: maximal open probability within the window range. Significance ($P < 0.05$) between CTR1 and each mutant clone was assessed by Student's *t*-test for unpaired measurements.

The delayed rectifier K^+ current (I_{Ks}), the late Na^+ current (I_{NaL}) and the pacemaker current (I_f) were recorded at physiological temperature by standard V-clamp protocols (detail in Supplementary material online). I_{Ks} and I_{NaL} were isolated as HMR1556 (1 μM)- and TTX (30 μM)-sensitive currents.

2.5 Intracellular Ca^{2+} measurements

Cytosolic Ca^{2+} and membrane current were simultaneously recorded in V-clamped hiPSC-CMs loaded with 10 μM Fluo4-AM; K^+ currents were blocked. Diastolic fluorescence was used as reference (F_0) for signal normalization (F/F_0) after subtraction of background. Ca^{2+} transients (CaT) were recorded during 300 ms steps to 0 mV (holding -50 mV), applied every 5 s.

Sarcoplasmic reticulum (SR) Ca^{2+} content (Ca_{SR}) was estimated by integrating the Na/Ca exchanger (NCX) current (I_{NCX}) elicited by 10 mM caffeine.[20] The slope of the I_{NCX}/Ca^{2+} relationship during the final third of the caffeine-induced transient was used to estimate NCX 'conductance'.[20]

The 'gain' of the coupling between membrane excitation and Ca^{2+} release was calculated as the ratio between CaT amplitude (F/F_0) and Ca^{2+} influx, obtained by integrating I_{CaL} up to the time of CaT peak.

The composition of experimental solutions is reported in the Supplementary material online.

2.6 Numerical simulations

Results of current clamp experiments were simulated *in silico* using a recently published hiPSC-CM AP model.[21] The I_{CaL} kinetic, as characterized in hiPSC-CMs in CTR1 and F142L was included into the model (see Supplementary material online). An additional amount of I_{K1}, based on the O'Hara–Rudy model of adult myocyte,[17] was incorporated in both CTR and F142L to mimic DC experimental conditions.

2.7 Statistics

Student's *t*-test or ANOVA for paired or unpaired measurements were applied as appropriate, with Bonferroni's correction in post-hoc comparisons. χ^2 statistics was used for comparison of categorical variables (GraphPad Prism 5). Data are expressed as mean ± SE; $P < 0.05$ defines significance, sample size is reported in figure legends.

3. Results

3.1 Characteristics of hiPSC-CMs donors

The proband under study is a young boy who suffered multiple syncopal events and cardiac arrest at the age of 14 years old. His QTc was very prolonged (between 600 and 700 ms) with episodes of T wave alternans often recorded by ECG Holter monitoring. When he was 9, mean HR was 66 b/min during the day, but at night HR dramatically dropped to less than 40 b/min. As compared with that of a normal subject, his QT/RR relationship was strongly non-linear, becoming significantly steeper at short RR intervals (see Supplementary material online, *Figure S3* and *Table S3*). Family history is unknown since he was adopted.

Two mutant hiPSC-CMs clones (c1 and c2) were obtained from patient's biopsy. Data from c1 and c2 are reported separately for I_{CaL} characterization (*Figure 2*) and, being closely comparable, have been pooled for the remaining studies. Because proband's relatives were unavailable, we used as healthy controls two genetically unrelated subjects: a 32-year-old Caucasian female (CTR1) and a 27-year-old Afro-American male (CTR2). For I_{CaL} characterization mutant hiPSC-CMs were compared to those of both CTR1 and CTR2; in the remaining studies CTR1 was used as control.

Molecular characterization of hiPSC-CMs demonstrated cardiomyocyte-like patterns of mRNA and protein expression (*Figure 1*), as also detailed in the Supplementary material online.

3.2 Transcriptional effects

To test for transcriptional changes secondary to the mutation, gene expression of CaM isoforms, ion channels, Ca^{2+} handling proteins and other Ca^{2+} binding proteins was analysed in CTR1 and mutant hiPSC-CMs. As shown in *Figure 1*, the mutation did not affect the expression of any of these genes (*Figure 1*). Also the levels of total CaM protein were

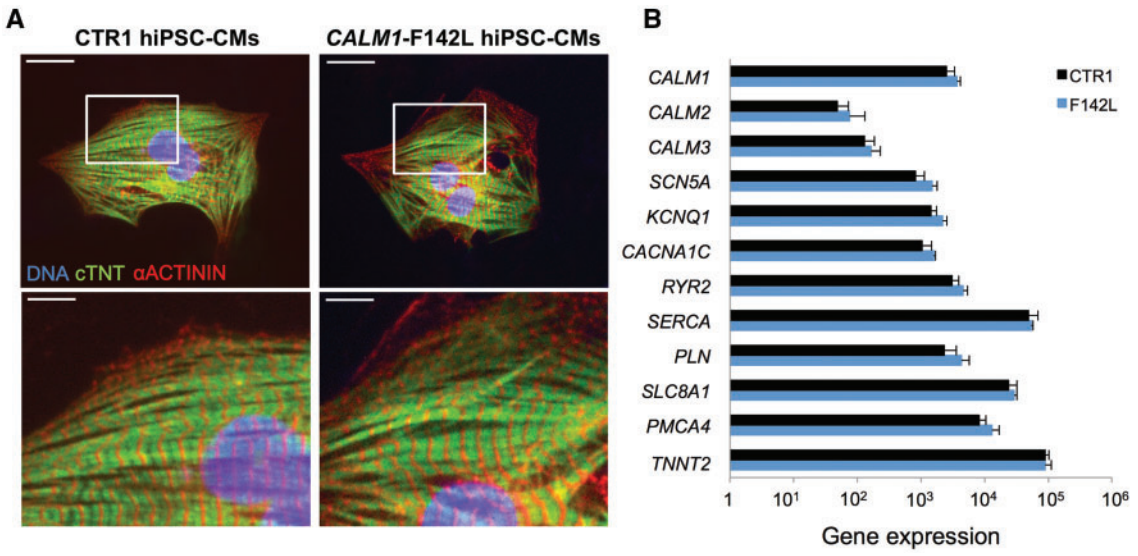

Figure 1 *CALM1*-F142L mutation does not affect the expression of CaM isoforms, ion channels and Ca^{2+} handling proteins. (*A*) Immunostaining for cardiac Troponin T (cTNT, green) and α-actinin (red) of CTR1 (left) and *CALM1*-F142L (right) hiPSC-CMs (nuclei in blue). Bottom panels are a magnification of the area framed in the upper images. (*B*) Quantitative RT-PCR analysis of *CALM* and cardiac-specific genes in CTR1 (black bars) and *CALM1*-F142L hiPSC-CMs (blue bars, clones c1 and c2 pooled). Data normalized to *GAPDH* and presented as mean ± SEM of three replicas. No significant differences were detected in the transcription pattern (Student's *t*-test for unpaired measurements). SCN5A: $Na_V1.5$ channel; KCNQ1: K^+ channel; CACNA1C: $Ca_V1.2$ channel; RyR2: Ryanodine receptor channel; SERCA: sarcoplasmic reticulum Ca^{2+} ATP-ase; PLN: phospholamban; SLC8A1: plasmalemmal Na^+/Ca^{2+} exchanger; PMCA4 plasmalemmal Ca^{2+} ATPase; TNNT2: troponinT.

similar in CTR1 and F142L hiPSC-CMs (see Supplementary material online, *Figure S4*).

3.3 Effects on I_{CaL} properties

We analysed I_{CaL} properties in c1 and c2 mutant hiPSC-CMs clones and in CTR1 hiPSC-CMs. In both mutant clones peak I_{CaL} density (*Figure 2A*) was similar to that of CTR1, but the sustained I_{CaL} component was significantly larger. In both mutant clones inactivation was positively shifted and incomplete, thus widening the voltage 'window' over which sustained I_{CaL} was present (*Table 1*). In mutant clones I_{CaL} inactivation was also slower than in CTR1 cells; as indicated by r_{100} and r_{300} values (*Figure 2*), this was due to weaker CDI. The wider 'window' and slower inactivation converged to enhance I_{CaL} sustained component in mutant hiPSC-CMs.

I_{CaL} recovery from inactivation is regulated by CaMKII[22] and relevant to I_{CaL} rate-dependency. Recovery time-course was tested for total I_{CaL} and after subtraction of the non-inactivating component (see Supplementary material online, *Figure S5*). As expected from defective CDI, a larger proportion of total I_{CaL} was available at short diastolic intervals in mutant hiPSC-CMs (see Supplementary material online, *Figure S5B*); when the inactivating component was analysed separately, recovery kinetics was similar between CTR1 and mutant cells (see Supplementary material online, *Figure S5C*). Recovery was faster, and the weight of the non-inactivating component smaller, at -80 mV than at -50 mV.

To rule out interindividual variability as a source of CDI differences, we analysed I_{CaL} properties in hiPSC-CMs from a second healthy control (CTR2) (see Supplementary material online, *Figure S6* and *Table S4*). Albeit in CTR2 I_{CaL} was larger and its properties were marginally different from those of CTR1, CDI and 'window' parameters were closely comparable.

CaMKII is a downstream signal mediating many effects of the Ca-CaM complex.[23] CaMKII activation was unexpectedly stronger in mutant hiPSC-CMs than in CTR1 ones (see Supplementary material online, *Figure S7*).

Rate-dependent and CaMKII-mediated I_{CaL} facilitation (CDF) can be detected in ventricular myocytes of different species.[24] However, CDF could not be induced even in CTR1 hiPSC-CMs (see Supplementary material online, *Figure S8A*). On the other hand, CDF was elicited by the same protocol in adult rat ventricular myocytes (see Supplementary material online, *Figure S8B*).

3.4 Effects on slow delayed rectifier K^+ current (I_{Ks}) and late Na^+ current (I_{NaL})

Given that both I_{Ks} and I_{NaL} are implicated in LQTS[25] and are modulated by CaM and/or CaMKII,[26,27] we analysed whether changes in these currents could contribute to this specific type of LQTS phenotype. As shown in *Figure 3A* and *B*, I_{Ks} *I–V* relationships and its steady-state activation were similar in CTR1 and mutant hiPSC-CMs. Non-inactivating components of I_{Na}, Na^+ 'window current' (I_{Naw}) and I_{NaL}, were evaluated by applying slow voltage ramps (*Figure 3C* and *D*) as previously reported.[28] TTX-sensitive current peaking at -38.0 ± 2.1 mV (CTR1, NS vs. F142L), mostly representing I_{Naw}, was less expressed in mutant cells, while no differences between groups were observed in the current activated at 0 mV, mostly representing I_{NaL}. Overall, in comparison to CTR1 hiPSC-CM, mutant cells showed smaller sustained I_{Na}, a finding opposite to what required to account for QT prolongation.

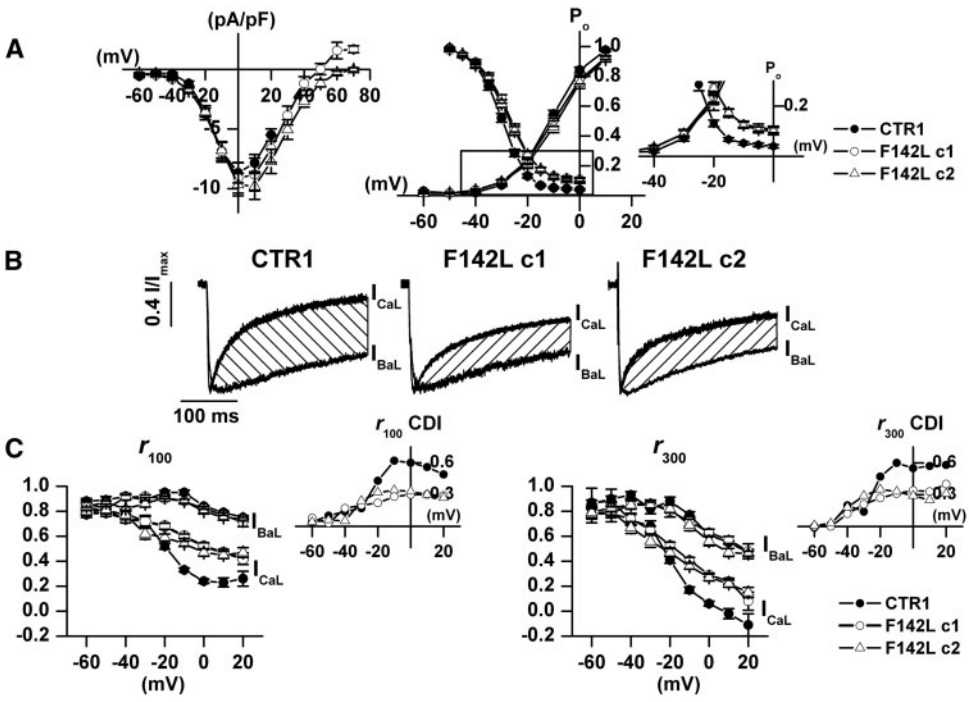

Figure 2 Steady-state I_{CaL} inactivation is positively shifted and CDI is reduced in *CALM1*-F142L hiPSC-CMs. I_{CaL} characterization in CTR1 (filled dots $N = 11$) and in the two *CALM1*-F142L clones (c1, open dots $N = 12$ and c2, open triangles $N = 13$) hiPSC-CMs separately. (*A*) *Left*: peak I_{CaL} I/V relationships; *Right*: I_{CaL} steady-state activation and inactivation curves; the 'window' range of potentials is zoomed in the inset (average data and statistics in *Table 1*). (*B*) I_{CaL} and I_{BaL} tracings recorded within the same cell at 0 mV; traces are normalized for their peak value; CDI was measured as the difference between I_{BaL} and I_{CaL} (dashed area). (*C*) Proportion of peak I_{CaL} and I_{BaL} remaining at 100 ms (r_{100}) and 300 ms (r_{300}), plotted as a function of the test potential. The insets show CDI as a function of test potential.

3.5 Effects on cardiac bodies and pacemaking

To reproduce tissue environment, field-potentials were recorded from spontaneously beating CBs at baseline and during β-adrenergic stimulation by isoproterenol (Iso 0.05–1.6 μM). The RR and QT intervals of CBs from the two mutant clones (c1 and c2) were similarly prolonged ($P < 0.05$ vs. CTR1, *Figure 4A*), reproducing both the bradycardic and LQTS phenotype of the patient. The relation between QT and RR intervals, evaluated by linear fitting (*Figure 4B*), was steeper in mutant CBs than in CTR1 ones (slope 0.22 ± 0.05 vs. 0.09 ± 0.02, $P < 0.05$) with a similar intercept. QTc was prolonged in mutant CBs (*Figure 4B*, inset). Isoproterenol effect on QT and RR saturated already at 0.05 μM and, at this concentration, it was larger in mutant than in CTR1 CBs (*Figure 4C*). Isoproterenol significantly increased QT/RR steepness in mutant CBs (*Figure 4D*, 0.49 ± 0.07, $P < 0.05$ vs. –Iso) while had no effect on CTR1 ones (*Figure 4D*, 0.08 ± 0.04, NS vs. –Iso).

Consistent with repolarization differences, contraction was more sustained and relaxation was slower in mutant CBs (see Supplementary material online, *Figure S9*).

In spite of the slow beating rate in mutant CBs, the pacemaker current (I_f) was grossly similar in CTR1 and F142L hiPSC CMs (see Supplementary material online, *Figure S10*). The I_f activation curve was slightly shallower in mutant cells (k from 7.7 to 9.7 mV, $P < 0.05$), a finding that can unlikely account alone for the huge difference in beating rate between groups.

3.6 Effect on electrical activity in isolated hiPSC-CMs

Mutation effects on AP repolarization and its rate-dependency were evaluated in hiPSC-CMs with ventricular-like APs (observed in > 80% of cells). The effect of DC on AP parameters is shown in Supplementary material online, *Figure S11*. Cells were studied under native conditions (see Supplementary material online, *Figure S12*) and during I_{K1} injection via DC (*Figure 5*). I_{K1} injection resulted in 'mature', ventricular-like AP contours, reduced AP duration (APD) variability and highlighted mutation-induced differences. Under DC, mutant hiPSC-CMs had significantly longer APD compared to CTR1 at all pacing rates below 3.3 Hz (*Figure 5A* and *B*). Whereas injected I_{K1} density during diastole was similar between control and mutant hiPSC-CMs, peak I_{K1} during the late AP repolarization phase was smaller in mutant ones, particularly at low pacing rate (see Supplementary material online, *Figure S13*), probably as a consequence of shallower AP repolarization in these cells[29] (see Supplementary material online).

In 20% of mutant cells, stimulation at 2 Hz induced APD alternans, which was never observed in CTR1 ones. At 3.3 Hz, 10% of CTR1 cells and 50% of mutant ones ($P < 0.05$, *Figure 5C* and *D*) could not follow stimulation because of failure of APD to shorten adequately. Numerical simulations showed that, at variance with the normal model, in the mutant one APD failed to adapt to 3.3 Hz pacing rate (mF142L trace in *Figure 5E*). Notably, the defect in I_{CaL} CDI was alone sufficient to account for the abnormality (mF142L CDIonly trace in *Figure 5E*). After

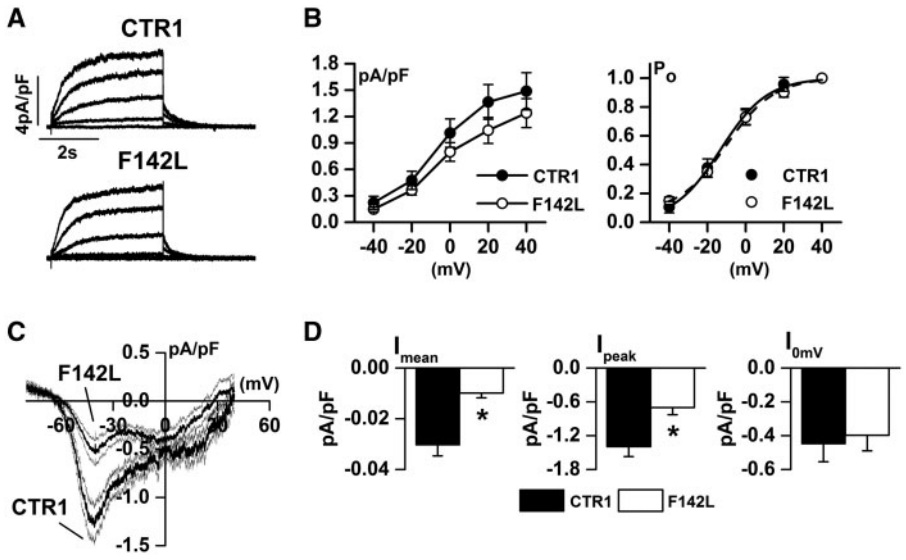

Figure 3 Steady-state I_{Ks} activation is unchanged and sustained I_{Na} is reduced in *CALM1*-F142L hiPSC-CMs. (*A*) HMR1556 (1 μM)-sensitive current (I_{Ks}) activated during voltage steps from a holding potential of - 40 mV in CTR1 and *CALM1*-F142L hiPSC-CMs. (*B*) I_{Ks} I/V relationships and steady state activation curves; Boltzmann fittings are represented by continuous and dashed lines for CTR1 ($N = 19$) and CALM1-F142L ($N = 25$) hiPSC-CMs respectively. (*C*) TTX (30 μM)-sensitive current (I_{TTX}) activated during slow voltage ramps (28 mV/sec) from a holding potential of - 100 mV, mean traces and SEM are shown. (*D*) Statistics for mean I_{TTX} (I_{mean}), peak I_{TTX} (I_{peak}, representative of I_{Naw}) and I_{TTX} activated at 0 mV (representative of I_{NaL}). CTR1: $N = 14$, *CALM1*-F142L: $N = 13$. $^*P < 0.05$ vs. CTR1 (Student's *t*-test for unpaired measurements).

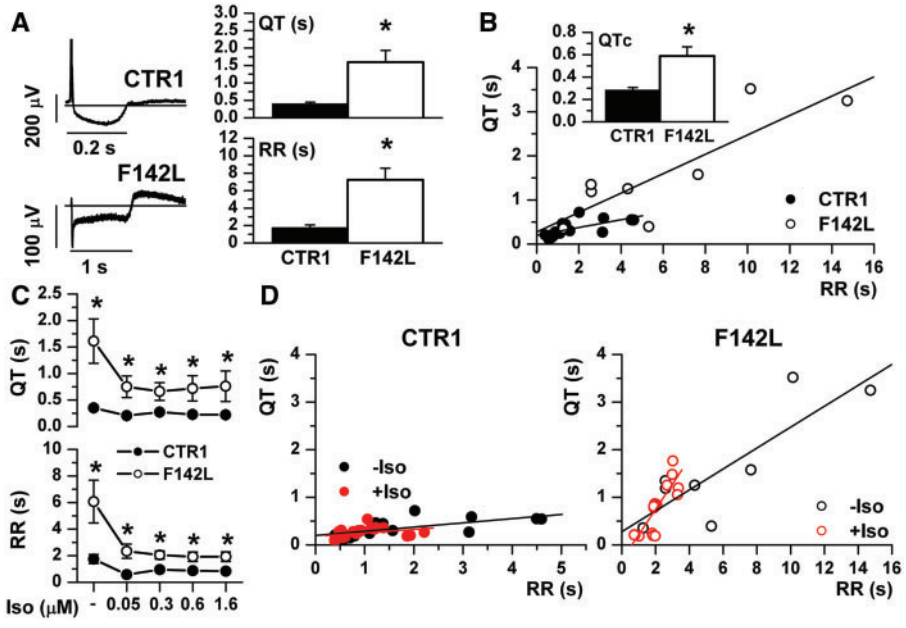

Figure 4 *CALM1*-F142L CBs show prolonged QTc and higher sensitivity to isoproterenol than CTR1 CBs. (*A*) *Left*: examples of field potentials from CTR1 and *CALM1*-F142L CBs. Arrows mark timepoints for QT measurement. *Right*: Statistics for QT and RR intervals (CTR1 $N = 18$, *CALM1*-F142L $N = 8$, data from mutant clones c1 and c2 pooled) under basal conditions. (*B*) QT-RR relationship; QTc statistics in the inset.). (*C*) Modulation of QT and RR by isoproterenol (Iso) ($N > 5$ at all concentrations in both groups). (*D*) QT-RR relationships at baseline (-Iso; black symbols) and during increasing Iso concentrations (+Iso red symbols) in CTR1 (left) and *CALM1*-F142L (right) CBs. $^*P < 0.05$ vs. CTR1 (Student's *t*-test for unpaired measurements).

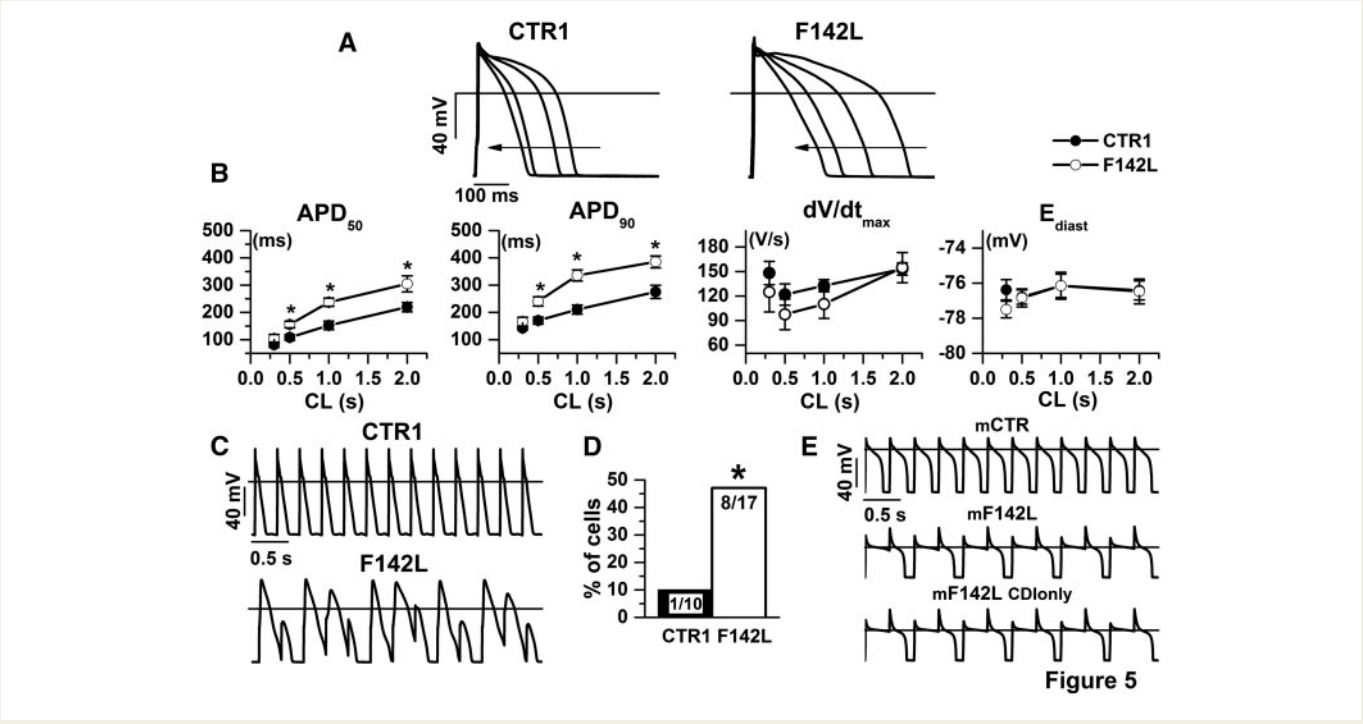

Figure 5 Isolated *CALM1*-F142L hiPSC-CMs show prolonged APD and failure of APD to shorten at high pacing rates, a finding reproduced by numerical simulations. (*A*) Action potential recorded at different pacing rates under DC; arrows indicate the direction of rate increase. (*B*) Statistics for APD_{50}, APD_{90}, dV/dt_{max} and E_{diast} in CTR1 (filled dots, $N \geq 6$) and *CALM1*-F142L (open dots, $N \geq 10$) (*$P < 0.05$ vs. CTR1, two-way ANOVA with Bonferroni's correction). The point at the shortest CL (rate = 3.3 Hz) refers only to cells that followed pacing (see text and panel D). (*C*) Sequences of action potentials evoked at 3.3 Hz in a CTR1 (top) and a *CALM1*-F142L (bottom) hiPSC-CMs. (*D*) Percentage of cells failing to follow pacing at 3.3 Hz. *$P < 0.05$ vs. CTR1 (χ^2 test). (*E*) Model (m) based simulation of the experimental protocol of panel C in CTR (top), *CALM1*-F142L (middle) and when only the F142L-related CDI reduction was incorporated into the computational model (bottom).

potentials, which would suggest spontaneous Ca^{2+} release events, were not observed, even at the highest pacing rate.

Cells studied under native conditions showed a qualitatively similar pattern (see Supplementary material online, *Figure S12*); however, mutation-induced differences were less pronounced and partially obscured by intercellular variability.

3.7 Effect on intracellular Ca^{2+} handling

CaM participates in the regulation of intracellular Ca^{2+} dynamics[8] which, in turn, may affect electrical stability.[30]

CaT amplitude was larger in mutant hiPSC-CMs than in CTR1 cells, however, because Ca^{2+} influx through I_{CaL} was also increased, the excitation-release (ER)-gain was unchanged (*Figure 6A-B*). In spite of the large difference in sarcolemmal Ca^{2+} influx, SR Ca^{2+} content was not affected by the mutation (*Figure 6C-E*). The kinetics of Ca^{2+} decay during the caffeine pulse (τ decay 1.88 ± 0.26 s vs. 1.93 ± 0.35 s, NS) and NCX 'conductance', were also similar between mutant and CTR1 cells (*Figure 6E*).

3.8 Pharmacological induction and rescue of the LQT phenotype

Failure of I_{CaL} CDI was pharmacologically induced by buffering subsarcolemmal Ca^{2+}. CTR1 and F142L hiPSC-CMs were incubated with the membrane permeable Ca^{2+} chelator BAPTA-AM (5 μM) for about 45 min. As shown in *Figure 7A*, at low pacing rates the repolarization was dramatically prolonged and unstable in both cell types; early after depolarizations (EADs) occurred and APD adaptation failed in most of cells at 2 Hz. Overall, removal of CDI by Ca^{2+} chelation abolished differences between CTR and mutant cells.

Rescue of LQTS phenotype was then tested by analysing the sensitivity of repolarization to verapamil and amlodipine in CBs by MEA recordings. Verapamil 50 nM shortened QTc significantly in mutant CBs, but had no effect on CTR1 ones (*Figure 7B*). Also amlodipine shortened QTc in mutant CBs (see Supplementary material online, *Figure S14*), but only at ≥900 nM, i.e. well above the EC_{50} for inhibition of contraction (10 nM).[31]

4. Discussion

The present work provides functional characterization of F142L-CaM in hiPSC-CMs derived from a symptomatic mutation carrier. The experimental strategy allowed to identify derangements, and relate them to clinical manifestations, in the context of native allelic balance and in the presence of all the factors, which might affect mutation expressivity. The mutation affected I_{CaL} time-course in a way consistent with delayed repolarization, the hallmark of the syndrome. I_{Ks} was unaffected and sustained I_{Na} was even smaller in mutant cells. Handling of intracellular Ca^{2+} was not directly altered, thus suggesting that the arrhythmogenic potential of this mutation may primarily reside in the electrophysiological

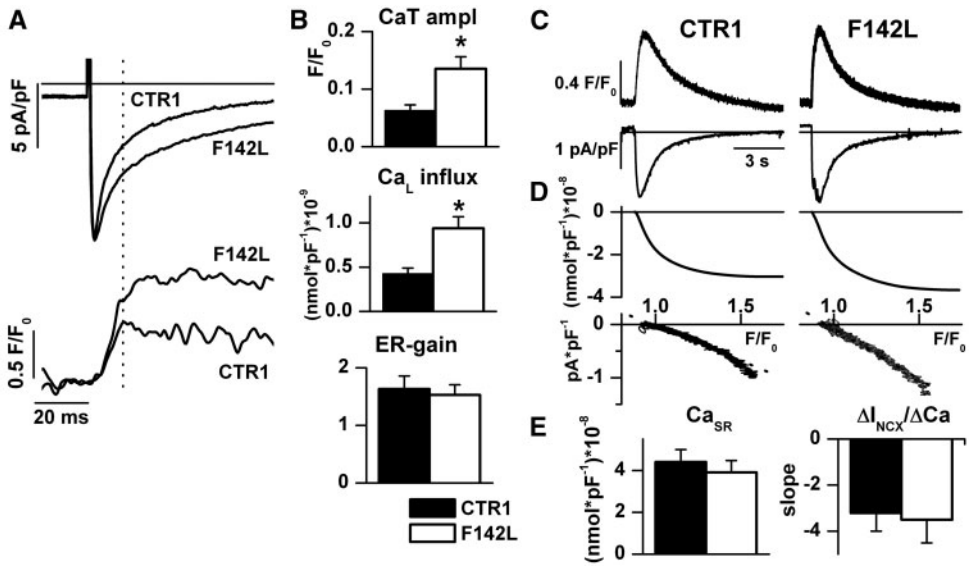

Figure 6 Intracellular Ca^{2+} handling and Ca^{2+} store stability are not significantly altered in V-clamped *CALM1*-F142L hiPSC-CMs. (*A*) Examples of I_{CaL} (top) and Ca^{2+} transients (CaT, bottom), evoked by voltage steps from -50 mV to 0 mV. Ca^{2+} influx (Ca_L) was measured from I_{CaL} up to the CaT peak (dotted line, see methods). (*B*) Statistics of CaT amplitude, Ca_L, and their ratio (ER-gain, see methods) in CTR1 ($N > 12$) and *CALM1*-F142L ($N > 9$; c1 and c2 pooled). (*C*) Caffeine-induced Ca^{2+} and current (I_{NCX}) transients (at - 50 mV). (*D*) Cumulative I_{NCX} integrals (top, used to estimate Ca_{SR}) and plots of I_{NCX} vs Ca^{2+} (bottom, slope used to estimate NCX 'conductance'). (*E*) Statistics for SR Ca^{2+} content (Ca_{SR}) and slope of I_{NCX}/Ca^{2+} relations in CTR1 ($N = 12$) and *CALM1*-F142L ($N = 13$, clones pooled) hiPSC-CMs. *$P < 0.05$ vs. CTR1 (Student's *t*-test for unpaired measurements).

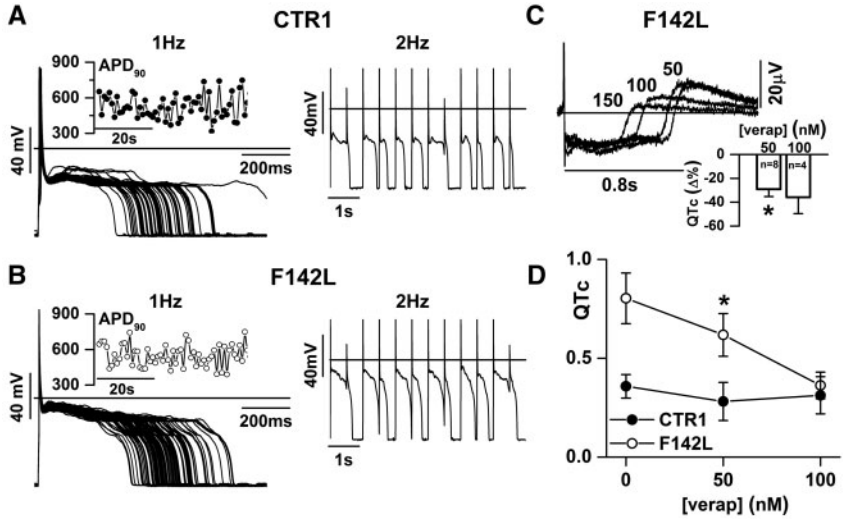

Figure 7 Intracellular Ca^{2+} buffering induces prolonged and unstable APDs in both *CALM1*-F142L and CTR1 hiPSC-CMs; verapamil shortens QTc in *CALM1*-F142L CBs only. Sequences of action potentials recorded at 1 Hz (left panels) or 2 Hz (right panels) in CTR1 (*A*) and *CALM1*-F142L (*B*) hiPSC-CMs pre-incubated with BAPTA-AM (5 μM). APD instability at 1 Hz is highlighted in insets; failing of APD to adapt at 2 Hz is shown on the right. Similar findings were observed in the majority of treated hiPSC-CMs (CTR1: 5 of 6, *CALM1*-F142L: 5 of 7). (*C*) Dose-dependent effects of verapamil on the field potential of a *CALM1*-F142L CB; tracings at various verapamil concentrations (numbers) are aligned on the time axis. Comparison of QTc shortening (Δ% from baseline) by verapamil at 50 and 100 nM respectively ($N \geq 4$, clones pooled). (*D*) Concentration-dependency of verapamil effect on QTc in CTR1 ($N \geq 5$) and *CALM1*-F142L CBs. *$P < 0.05$ vs. baseline (Student's *t*-test for paired measurements).

abnormality. Even in the presence of the native allelic balance, F142L-CaM caused marked CDI abnormality to imply strong negative dominance of the mutant protein.

4.1 Target specificity and negative dominance

Beside $Ca_v1.2$ channels, also $K_v7.1$ channels, responsible for I_{Ks}, require functional CaM for their correct assembly and gating.[26] Heterologous F142L CaM mutation did not affect I_{Ks}, thus implying compensation by wild-type CaM.

Moreover, ryanodine receptor (RyR) channels and CaMKII are direct downstream CaM targets. As suggested by unchanged ER-gain and SR Ca^{2+} content (*Figure 6*), the mutation did not cause RyRs instability, which would be expected from loss of modulation by CaM.[8] The latter would also be expected to reduce CaMKII activity, which was nevertheless increased in mutant hiPSC-CMs.[10] On the other hand, CDI was strongly impaired by a mutation affecting only 1/6 of CaM alleles. Altogether, these findings imply that mutant CaM selectively interacts with $Ca_v1.2$ with strong negative dominance. Both selectivity and negative dominance may be interpreted by considering that modulation of $Ca_v1.2$ is mediated by a pre-bound apoCaM pool, formed independent of Ca^{2+}-induced activation.[32] Because of its increased affinity for $Ca_v1.2$ channels,[12] mutant apoCaM may dominate the pre-bound pool even in the presence of the unfavourable concentration ratio. CaM also binds RyR2 as apoCaM,[33] but heterologous expression studies suggest that high affinity Ca^{2+} binding to CaM C-lobe is essential for diastolic RyR2 stabilization.[34] Therefore, rather than reflecting irrelevance of F142L to RyR2 gating, normal RyRs function may result from compensation by wild-type CaM. The latter likely accounts also for lack of negative effects on CaMKII; the observed increase in CaMKII activity may simply be secondary to CDI impairment, i.e. reflect upregulation of residual wild-type CaM-CaMKII complexes by enhanced Ca^{2+} influx.

Phosphorylation by CaMKII may facilitate opening of RyRs[35] and $Ca_V1.2$ channels (Ca^{2+} -induced I_{CaL} facilitation, CDF),[8,22] and destabilize $Na_v1.5$ channel inactivation (I_{NaL} enhancement).[27] RyR facilitation, if present, was not large enough to be functionally relevant. I_{CaL} facilitation (CDF) was absent even in control hiPSC-CMs (see Supplementary material online, *Figure S8*). The present data provide the first comparative measurement of I_{CaL} CDF in human and rodent cells; nevertheless, the absence of the phenomenon in the former might also reflect hiPSC-CMs immaturity (e.g. lack of T-tubules).[36] Therefore, the present observation should not be considered conclusive for the absence of I_{CaL} facilitation in mature human cardiomyocytes.

Moreover, I_{NaL} was unaffected and I_{Naw} was even decreased in mutant hiPSC-CMs; thus, changes in these currents are unlikely to contribute to mutation-induced QT prolongation. CaMKII activity was found to be enhanced in F142L hiPSC-CMs, but still inadequate to induce the expected functional changes (RyR and I_{CaL} facilitation, I_{NaL} enhancement).

Defective CDI and prolonged repolarization might increase SR Ca^{2+} content, which was instead unaffected by the mutation (*Figure 6E*). While this might reflect adaptive upregulation of Ca^{2+} efflux, NCX 'conductance' was unchanged (*Figure 6D* and *E*) and, at least at transcriptional level, other Ca^{2+} transports were also unmodified (*Figure 1*). Therefore, we propose that, under the present conditions, the functional reserve of existing NCX, recruited by the larger Ca^{2+} transients, was adequate to balance the extra Ca^{2+} influx. This interpretation is consistent with previous work showing that Ca_{SR} is largely independent of sarcolemmal Ca^{2+} influx.[37]

4.2 Reproduction of clinical phenotype and pro-arrhythmic mechanism

The mutation carrier had prolonged QTc and a markedly non-linear QT/RR relationship, reflecting enhanced QT rate-dependency during tachycardia which, in turn, likely mirrors sympathetic activation. All these features were also present in mutant CBs (and hiPSC-CMs), in which QTc was prolonged, QT/RR (and APD/CL) relation was steeper and abnormally sensitive to isoproterenol. T wave alternans also occurred in the patient, possibly matching the higher incidence of repolarization irregularities in mutant hiPSC-CMs.

As most LQTS patients, the proband was bradycardic and this was reproduced *in vitro* by measuring spontaneous rate in CBs. Pacemaking can originate from pacemaker current (I_f) and/or from an intracellular Ca^{2+} clock.[38] I_f was comparable between control and mutant hiPSC-CMs and, if anything, we would expect increased Ca^{2+} influx to accelerate a Ca^{2+} clock. Therefore, by exclusion, we speculate that the low beating rate may be due to APD prolongation.

The present data point to inadequate CDI, and the resulting repolarization abnormality, as the primary cause of arrhythmias; indeed, failure of ER-gain to change in the presence of constant Ca_{SR} argues against primary SR instability.

Because of homeostatic regulation of intracellular Ca^{2+}, Ca_{SR} may be rather insensitive to changes in sarcolemmal Ca^{2+} influx[37]; therefore, failure of Ca_{SR} to increase significantly is not surprising. Nevertheless, Ca_{SR} was measured here under V-clamp, a condition not representative of in-vivo electrical activity; we cannot rule out that prolonged repolarization might change the Ca^{2+} influx/efflux balance at short cycle lengths. Limpitikul et al.[12] found *CALM-F142L* overexpression to increase Ca_{SR} in guinea-pig myocytes even at very low pacing rates (0.1 Hz) and suggested instead that SR instability might contribute to arrhythmogenesis. Notably, these experiments were performed at room temperature, at which myocytes were incompletely polarized and had extremely slow repolarization; such conditions are clearly inadequate to provide information on Ca^{2+} influx/efflux balance *in vivo*. On the other hand, Yin *et al.*[11] reported unchanged Ca_{SR} at 1 Hz in foetal murine myocytes. Whether or not the mutation may result in intracellular Ca^{2+} overload, the complete absence of afterpotentials in I-clamp recordings (even at high pacing rates), argues against SR instability as a mechanism contributing to arrhythmogenesis.

Repolarization was affected by two apparently antithetical abnormalities. In a large fraction of mutant isolated hiPSC-CMs, APD failed to shorten at high rates (3.3 Hz, *Figure 5D*), likely because of abnormal persistence of I_{CaL} availability (see Supplementary material online, *Figure S5*); this caused failure, or major distortion of subsequent excitations (*Figure 5C*). This defect was not observed in mutant CBs (*Figure 4*), possibly because delayed repolarization limited spontaneous beating rate. The second abnormality consisted of steeper QT/RR and APD/CL relations (*Figures 4 and 5*). Strong rate-dependency of repolarization is known to entail proarrhythmic risk.[39] APD prolongation on its own causes steeper APD rate-dependency,[29] but defective CDI might contribute to enhance sensitivity to β-adrenergic stimulation.

Simulation results confirmed that failure of APD adaptation to high pacing rates occurs in the presence of defective CDI of I_{CaL}. Separation of the CDI defect from the other abnormalities detected in F142L hiPSC-CMs suggest that the former alone is adequate to account for the phenotype (*Figure 5E*).

4.3 Clinical implications

The present results suggest that, in the case of *CALM1*-F142L, arrhythmogenesis may strictly result from the effect of excess I_{CaL} on repolarization. If this is the case, I_{CaL} blockade may be a logical therapeutic approach. The observation that verapamil reversed the mutation phenotype is consistent with this view. Thus, the identification of the arrhythmogenic mechanisms in the context of patient's genotype may enable the development of tailored therapeutic strategies.

Previous studies found QT-prolonging CaM mutations (e.g. D130G) to impair the ability of foetal murine cells to follow pacing even at slow rates.[11] This potentially arrhythmogenic feature was reversed by β-adrenergic stimulation, which was thus suggested as a therapeutic approach.[11] However, this abnormality was rare in the case of F142L-CaM[11] and, also in the present study, occurred at high rates only. On the other hand, enhanced sensitivity of repolarization to β-adrenergic stimulation might entail proarrhythmic risk.[39] Therefore, the present data do not support the view that β-adrenergic stimulation may represent a therapeutic approach, at least in the case of F142L-CaM.

4.4 Study limitations

A limitation in modelling arrhythmogenic syndromes with hiPSC-CM is represented by the degree of maturity of these cells, which often are more similar to foetal rather than adult CMs. Low I_{K1} expression is an important aspect of electrical immaturity, which we compensated by I_{K1} injection (DC technique). Other aspects of immaturity could not be corrected; consequently, extrapolation of our results should be done with caution.

Isogenic control hiPSC-CMs were not available for this study. To provide a comparison adequate to identify mutation-induced abnormalities, the opposite strategy of using multiple controls with maximal genetic heterogeneity was adopted. To this end, two iPSC-CMs control lines were generated from healthy donors with different gender and ethnicity, factors known to be involved in setting channels expression and AP duration. Except for different peak I_{CaL} magnitude, a complete consistency between CTR cell lines was found in I_{CaL} properties relevant to repolarization course, such as window current and CDI. This sharply contrasts with the obvious abnormality in the persistent I_{CaL} component observed in F142L hiPSC-CMs.

Generalization of the mechanisms identified in the present study to all cases of the F142L CaM mutation is limited by the fact that all mutant cell lines originated from a single mutation carrier.

Supplementary material

Supplementary material is available at *Cardiovascular Research* online.

Acknowledgements

The Authors are grateful to Dr Gabi Lederer (Cytogenetic Department, Technical University Munich) for providing karyotype data, and to Dr Vlasta Bari (Department of Biomedical Sciences for Health, University of Milan, Milan, Italy) for analysing 24 h Holter recordings.

Conflict of interest: none declared.

Funding

This work was supported by grants from the Italian Ministry of University and Research (MIUR-PRIN 2010BWY8E9_005 to G.M. and R.M.), Italian Ministry of Health (GR-2010-2305717 to C.L. and M.G.), the German Research Foundation, Research Unit 923 (Mo 2217/1-1 to M.A. and Si 1747/1-1 to S.D.), and the Academic Research Fund (F.A.R Milano-Bicocca to Z.A.).

References

1. Schwartz PJ, Ackerman MJ, George AL, Jr, Wilde AA. Impact of genetics on the clinical management of channelopathies. *J Am Coll Cardiol* 2013;**62**:169–180.
2. Crotti L, Johnson CN, Graf E, De Ferrari GM, Cuneo BF, Ovadia M, Papagiannis J, Feldkamp MD, Rathi SG, Kunic JD, Pedrazzini M, Wieland T, Lichtner P, Beckmann BM, Clark T, Shaffer C, Benson DW, Kaab S, Meitinger T, Strom TM, Chazin WJ, Schwartz PJ, George AL, Jr. Calmodulin mutations associated with recurrent cardiac arrest in infants. *Circulation* 2013;**127**:1009–1017.
3. Marsman RF, Barc J, Beekman L, Alders M, Dooijes D, van den WA, Ratbi I, Sefiani A, Bhuiyan ZA, Wilde AA, Bezzina CR. A mutation in CALM1 encoding calmodulin in familial idiopathic ventricular fibrillation in childhood and adolescence. *J Am Coll Cardiol* 2014;**63**:259–266.
4. Makita N, Yagihara N, Crotti L, Johnson CN, Beckmann BM, Roh MS, Shigemizu D, Lichtner P, Ishikawa T, Aiba T, Homfray T, Behr ER, Klug D, Denjoy I, Mastantuono E, Theisen D, Tsunoda T, Satake W, Toda T, Nakagawa H, Tsuji Y, Tsuchiya T, Yamamoto H, Miyamoto Y, Endo N, Kimura A, Ozaki K, Motomura H, Suda K, Tanaka T, Schwartz PJ, Meitinger T, Kaab S, Guicheney P, Shimizu W, Bhuiyan ZA, Watanabe H, Chazin WJ, George AL, Jr. Novel calmodulin mutations associated with congenital arrhythmia susceptibility. *Circ Cardiovasc Genet* 2014;**7**:466–474.
5. Reed GJ, Boczek NJ, Etheridge SP, Ackerman MJ. CALM3 mutation associated with long QT syndrome. *Heart Rhythm* 2015;**12**:419–422.
6. Chin D, Means AR. Calmodulin: a prototypical calcium sensor. *Trends Cell Biol* 2000;**10**:322–328.
7. Fischer R, Koller M, Flura M, Mathews S, Strehler-Page MA, Krebs J, Penniston JT, Carafoli E, Strehler EE. Multiple divergent mRNAs code for a single human calmodulin. *J Biol Chem* 1988;**263**:17055–17062.
8. Saucerman JJ, Bers DM. Calmodulin binding proteins provide domains of local Ca^{2+} signaling in cardiac myocytes. *J Mol Cell Cardiol* 2012;**52**:312–316.
9. Nyegaard M, Overgaard MT, Sondergaard MT, Vranas M, Behr ER, Hildebrandt LL, Lund J, Hedley PL, Camm AJ, Wettrell G, Fosdal I, Christiansen M, Borglum AD. Mutations in calmodulin cause ventricular tachycardia and sudden cardiac death. *Am J Hum Genet* 2012;**91**:703–712.
10. Hwang HS, Nitu FR, Yang Y, Walweel K, Pereira L, Johnson CN, Faggioni M, Chazin WJ, Laver D, George AL, Jr., Cornea RL, Bers DM, Knollmann BC. Divergent regulation of ryanodine receptor 2 calcium release channels by arrhythmogenic human calmodulin missense mutants. *Circ Res* 2014;**114**:1114–1124.
11. Yin G, Hassan F, Haroun AR, Murphy LL, Crotti L, Schwartz PJ, George AL, Satin J. Arrhythmogenic calmodulin mutations disrupt intracellular cardiomyocyte Ca^{2+} regulation by distinct mechanisms. *J Am Heart Assoc* 2014;**3**:e000996.
12. Limpitikul WB, Dick IE, Joshi-Mukherjee R, Overgaard MT, George AL, Jr., Yue DT. Calmodulin mutations associated with long QT syndrome prevent inactivation of cardiac L-type Ca(2+) currents and promote proarrhythmic behavior in ventricular myocytes. *J Mol Cell Cardiol* 2014;**74**:115–124.
13. Gramlich M, Pane LS, Zhou Q, Chen Z, Murgia M, Schotterl S, Goedel A, Metzger K, Brade T, Parrotta E, Schaller M, Gerull B, Thierfelder L, Aartsma-Rus A, Labeit S, Atherton JJ, McGaughran J, Harvey RP, Sinnecker D, Mann M, Laugwitz KL, Gawaz MP, Moretti A. Antisense-mediated exon skipping: a therapeutic strategy for titin-based dilated cardiomyopathy. *EMBO Mol Med* 2015;**7**:562–576.
14. Erickson JR, Patel R, Ferguson A, Bossuyt J, Bers DM. Fluorescence resonance energy transfer-based sensor Camui provides new insight into mechanisms of calcium/calmodulin-dependent protein kinase II activation in intact cardiomyocytes. *Circ Res* 2011;**109**:729–738.
15. Liang P, Lan F, Lee AS, Gong T, Sanchez-Freire V, Wang Y, Diecke S, Sallam K, Knowles JW, Wang PJ, Nguyen PK, Bers DM, Robbins RC, Wu JC. Drug screening using a library of human induced pluripotent stem cell-derived cardiomyocytes reveals disease-specific patterns of cardiotoxicity. *Circulation* 2013;**127**:1677–1691.
16. Doss MX, Di Diego JM, Goodrow RJ, Wu Y, Cordeiro JM, Nesterenko VV, Barajas-Martinez H, Hu D, Urrutia J, Desai M, Treat JA, Sachinidis A, Antzelevitch C. Maximum diastolic potential of human induced pluripotent stem cell-derived cardiomyocytes depends critically on I(Kr). *PLoS One* 2012;**7**:e40288.
17. O'Hara T, Virag L, Varro A, Rudy Y. Simulation of the undiseased human cardiac ventricular action potential: model formulation and experimental validation. *PLoS Comput Biol* 2011;**7**:e1002061.
18. Meijer van Putten RM, Mengarelli I, Guan K, Zegers JG, Van Ginneken AC, Verkerk AO, Wilders R. Ion channelopathies in human induced pluripotent stem cell derived cardiomyocytes: a dynamic clamp study with virtual IK1. *Front Physiol* 2015;**6**:7.
19. Bartolucci C, Altomare C, Bennati M, Furini S, Zaza A, Severi S. Combined action potential- and dynamic-clamp for accurate computational modelling of the cardiac IKr current. *J Mol Cell Cardiol* 2015;**79**:187–194.
20. Rocchetti M, Alemanni M, Mostacciuolo G, Barassi P, Altomare C, Chisci R, Micheletti R, Ferrari P, Zaza A. Modulation of sarcoplasmic reticulum function by

PST2744 [istaroxime; (E,Z)-3-((2-aminoethoxy)imino) androstane-6,17-dione hydrochloride)] in a pressure-overload heart failure model. *J Pharmacol Exp Ther* 2008;**326**:957–965.
21. Paci M, Hyttinen J, Rodriguez B, Severi S. Human induced pluripotent stem cell-derived versus adult cardiomyocytes: an in silico electrophysiological study on effects of ionic current block. *Br J Pharmacol* 2015;**172**:5147–5160.
22. Guo J, Duff HJ. Calmodulin kinase II accelerates L-type Ca2+ current recovery from inactivation and compensates for the direct inhibitory effect of [Ca2+]i in rat ventricular myocytes. *J Physiol* 2006;**574**:509–518.
23. Maier LS, Bers DM. Role of Ca2+/calmodulin-dependent protein kinase (CaMK) in excitation-contraction coupling in the heart. *Cardiovasc Res* 2007;**73**:631–640.
24. Bers DM, Morotti S. Ca(2+) current facilitation is CaMKII-dependent and has arrhythmogenic consequences. *Front Pharmacol* 2014;**5**:144.
25. Schwartz PJ, Crotti L, Insolia R. Long-QT syndrome: from genetics to management. *Circ Arrhythm Electrophysiol* 2012;**5**:868–877.
26. Shamgar L, Ma L, Schmitt N, Haitin Y, Peretz A, Wiener R, Hirsch J, Pongs O, Attali B. Calmodulin is essential for cardiac IKS channel gating and assembly: impaired function in long-QT mutations. *Circ Res* 2006;**98**:1055–1063.
27. Wagner S, Dybkova N, Rasenack EC, Jacobshagen C, Fabritz L, Kirchhof P, Maier SK, Zhang T, Hasenfuss G, Brown JH, Bers DM, Maier LS. Ca^{2+}/calmodulin-dependent protein kinase II regulates cardiac Na^{+} channels. *J Clin Invest* 2006;**116**:3127–3138.
28. Rocchetti M, Sala L, Rizzetto R, Staszewsky LI, Alemanni M, Zambelli V, Russo I, Barile L, Cornaghi L, Altomare C, Ronchi C, Mostacciuolo G, Lucchetti J, Gobbi M, Latini R, Zaza A. Ranolazine prevents INaL enhancement and blunts myocardial remodelling in a model of pulmonary hypertension. *Cardiovasc Res* 2014;**104**:37–48.
29. Zaza A. Control of the cardiac action potential: the role of repolarization dynamics. *J Mol Cell Cardiol* 2010;**48**:106–111.
30. Zaza A, Rocchetti M. Calcium store stability as an antiarrhythmic endpoint. *Curr Pharm Des* 2015;**21**:1053–1061.
31. Jeppesen P, Bruun J, Nielsen-Kudsk F. Amlodipine dynamic effects and myocardial pharmacokinetics in the isolated and perfused guinea-pig heart. *Pharmacol Toxicol* 1998;**82**:250–256.
32. Erickson MG, Liang H, Mori MX, Yue DT. FRET two-hybrid mapping reveals function and location of L-type Ca^{2+} channel CaM preassociation. *Neuron* 2003;**39**:97–107.
33. Yamaguchi N, Xu L, Pasek DA, Evans KE, Meissner G. Molecular basis of calmodulin binding to cardiac muscle Ca(2+) release channel (ryanodine receptor). *J Biol Chem* 2003;**278**:23480–23486.
34. Sondergaard MT, Tian X, Liu Y, Wang R, Chazin WJ, Chen SR, Overgaard MT. Arrhythmogenic calmodulin mutations affect the activation and termination of cardiac ryanodine receptor-mediated Ca^{2+} release. *J Biol Chem* 2015;**290**:26151–26162.
35. Anderson ME. CaMKII and a failing strategy for growth in heart. *J Clin Invest* 2009;**119**:1082–1085.
36. Gherghiceanu M, Barad L, Novak A, Reiter I, Itskovitz-Eldor J, Binah O, Popescu LM. Cardiomyocytes derived from human embryonic and induced pluripotent stem cells: comparative ultrastructure. *J Cell Mol Med* 2011;**15**:2539–2551.
37. Trafford AW, Diaz ME, Eisner DA. Coordinated control of cell Ca(2+) loading and triggered release from the sarcoplasmic reticulum underlies the rapid inotropic response to increased L-type Ca(2+) current. *Circ Res* 2001;**88**:195–201.
38. Mangoni ME, Nargeot J. Genesis and regulation of the heart automaticity. *Physiol Rev* 2008;**88**:919–982.
39. Gilmour RF, Jr. A novel approach to identifying antiarrhythmic drug targets. *Drug Discov Today* 2003;**8**:162–167.